



1

2 *PDO-driven interdecadal variability of snowfall over the Karakoram and Western Himalaya*

3

4

5 **Authors: Priya Bharati¹, Pranab Deb¹, Kieran M. R. Hunt^{2,3}**

6

7

8 **1 CORAL, Indian Institute of Technology Kharagpur, Kharagpur, India**

9 **2 Department of Meteorology, University of Reading, Reading, UK**

10 **3 National Centre for Atmospheric Science, University of Reading, UK**

11

12

13 *Correspondence to:* pranab@coral.iitkgp.ac.in

14

15

16

17

18

19

20

21

22

23

24

25

26

27

28

29

30

31



32

33 **Abstract:**

34 Our study reveals that the negative phase of the Pacific Decadal Oscillation (PDO-) leads to
35 increased winter (DJF) snowfall in the Karakoram and Western Himalayas (KH) from 1940 to
36 2022. Interdecadal variations in DJF snowfall during the PDO- are attributed to deep convection
37 and adiabatic cooling near the tropopause in both the northwest Pacific and KH region.
38 Additionally, a wave-like pattern characterized by a trough (anomalous cyclone) north of KH and a
39 ridge (anomalous Tibetan Plateau anticyclone) east of KH in the upper atmosphere, along the
40 northward shift of the DJF Subtropical Jet (STJ) was observed. A strong positive correlation
41 between DJF STJ strength and DJF snowfall in KH as well as a significant negative correlation
42 between DJF STJ strength and DJF PDO, suggests a wave response over KH to the direct forcing
43 over the northwest Pacific Ocean. The intensified STJ across KH results in higher frequency of
44 Western disturbances, leading to anomalous moisture convergence and increased DJF precipitation
45 in the region during the PDO-. These findings hold significant implications for the decadal
46 predictability of winter snowfall in KH by the various phases of PDO.

47

48 **1) Introduction:**

49 Glaciers in the Karakoram and Western Himalaya (KH) exhibit unique stability compared to other
50 alpine glaciers (known as the ‘Karakoram Anomaly’; Hewitt, 2005; Kaab et al., 2012; Gardelle et
51 al., 2013; Kapnick et al., 2014; Forsythe et al., 2017; de Kok et al., 2018; Farinotti et al., 2020;
52 HIMAP, 2020). Winter snowfall plays a significant role in preserving the local snowpack and
53 sustaining the glacial mass balance at higher elevations (Tahir et al., 2011; Bolch et al., 2012;
54 Ridley et al., 2013; Cannon et al., 2015; Dimri et al., 2015), and controls almost 60% of the
55 variability in glacier mass balance in the KH region (Kumar et al., 2019). The decline in average
56 and minimum summer temperatures, along with significant increases in winter, summer, and annual
57 precipitation, have been proposed as crucial factors influencing the stable glacier budget of the KH
58 in recent decades (Archer and Fowler, 2006; Forsythe et al., 2017).

59 The KH receives around 50% of its annual precipitation as snowfall from western disturbances
60 (WDs) (Lang and Barros, 2004; Barros et al., 2006; Bookhagen and Burbank, 2010; Hunt et al.,
61 2024). Furthermore, WDs account for more than 65% of all winter snowfall and nearly 53% of total
62 winter precipitation in the KH (Javed et al., 2022). However, using a less conservative method,
63 Midhuna et al. (2020) found that WDs account for about 80% of winter precipitation in KH. WDs



64 are upper level troughs in the subtropical westerly jet (STJ), which grow via baroclinic instability
65 (Norris et al., 2015; Cannon et al., 2017; Hunt et al., 2018). Strong WDs are associated with deep
66 uplift to the east of their centre and drive moist lower-tropospheric southwesterlies from the Arabian
67 Sea (Dimri and Dash, 2012; Hunt et al., 2018), resulting in heavy precipitation along the foothills
68 and mountains of KH region (Baudouin et al., 2020). The snowfall from WDs in the KH is heavily
69 influenced by the complex topography of the region, as well as by synoptic and mesoscale factors
70 (Cannon et al., 2015; Norris et al., 2015, 2017, 2018). Subsequent snowmelt in the following spring
71 and summer seasons and associated runoff serve as major sources of downstream river flow and
72 provide relief from drought to populations that are vulnerable to water stress (Bolch et al., 2012;
73 Hewitt et al., 2014; Rana et al., 2019; Pritchard et al., 2019).

74

75 However, the main climatic drivers affecting seasonal precipitation, and hence glacial mass balance
76 in the region are only partially understood (Cannon et al., 2015). WD activity during winter season
77 over the KH has been reported to be influenced by several global climate forcings such as North
78 Atlantic Oscillation/Arctic Oscillation (Yadav et al., 2009; Syed et al., 2010; Filippi et al., 2014;
79 Basu et al., 2017; Midhuna and Dimri, 2019; Hunt and Zaz, 2022), El Niño–Southern Oscillation
80 (ENSO) (Yadav et al., 2010; Dimri, 2013; Kar and Rana, 2014; Cannon et al., 2017; Kamil et al.,
81 2019; Rana et al., 2019; Bharati et al., 2024), Polar/Eurasian Pattern and Siberian High (Wu and
82 Wang, 2002; Cannon et al., 2014), Madden–Julian Oscillation (Barlow et al., 2005; Cannon et al.,
83 2017) and Indian Ocean Dipole (Yadav et al., 2007; Hoell et al., 2013) on intraseasonal and
84 interannual timescales. In particular, the ENSO exerts the strongest influence on the interannual
85 variability of winter precipitation in KH (Rana et al., 2019). One of the key aspects of ENSO
86 teleconnection to Indian Himalayas is the southward shift in the latitude of the winter STJ over the
87 KH during the positive phase of ENSO (Cannon et al., 2014, 2017), which leads to heavier WD
88 precipitation as their tracks move closer to their primary moisture source, the Arabian Sea (Bharati
89 et al., 2024).

90

91 Precipitation gauges in the Himalayas are sparse and recognised as inadequate for accurately
92 measuring snowfall (Anders et al., 2006; Rana et al., 2015). While satellite records of precipitation
93 are available, they cover only a limited time frame, whereas our study requires long-term data to
94 analyze the interdecadal variability of precipitation over the KH region. We currently have an 85-
95 year-long reanalysis from ERA5, which has demonstrated a high degree of similarity in both the



96 quantity and variability of winter precipitation across all time scales when compared to observations
97 and satellite data in the KH region (Baudouin et al., 2020). The long dataset from ERA5 is
98 sufficient to examine the interdecadal variability of DJF snowfall over KH. The low-frequency
99 modes of atmospheric variability such as the Pacific Decadal Oscillation (PDO), Inter-decadal
100 Pacific Oscillation (Mantua et al., 1998; Zhang et al., 1997; Power et al., 1999; Dai, 2013), and the
101 Atlantic Multi-decadal Oscillation (Enfield et al., 2001) are known to modulate the regional climate
102 of the Northern Hemisphere over inter-decadal to multi-decadal timescales. Among these, the PDO
103 is the dominant mode of SST oscillation in the North Pacific, influencing long-term precipitation
104 patterns globally (Dettinger et al., 1998; Krishnamurthy, 2013, 2014; Wang et al., 2014; Dong and
105 Dai, 2015; Yang et al., 2017; Wu and Mao, 2016; Qin et al., 2017). For example, Indian monsoon
106 rainfall and autumn precipitation in North Central China were found to show an inverse relationship
107 with PDO (Krishnan and Sugi, 2003; Krishnamurthy, 2014; Qin et al., 2017). However, there is a
108 major gap in understanding how the PDO affects precipitation over any parts of Himalayas during
109 any of the seasons.

110

111 The current study aims to address this knowledge gap by examining the modulation of the
112 interdecadal variability of winter snowfall over KH by PDO. Our study aims to understand the
113 potential influence of the PDO on the Karakoram anomaly, which deviates from the general climate
114 change patterns observed in the KH region and other mountainous areas. The main objective of this
115 study are: (1) To examine the spatial distribution of decadal snowfall in KH in different phases of
116 PDO, (2) how the PDO adjusts global circulation patterns, leading to changes in the STJ, and (3)
117 how these changes cause impact on a local scale over the KH through WDs and moisture transport.

118

119 **2) Data and Methods:**

120 **2.1 Data**

121 **2.1.1) Meteorological data**

122 The study uses meteorological data including geopotential height, zonal (u) and meridional wind (v)
123 at 200 hPa level, vertically averaged temperature from 500 to 300 hPa level, vertically integrated
124 moisture flux (VIMF), vertically integrated moisture flux convergence (VIMFC), and global sea
125 surface temperature (SST) obtained from the European Centre for Medium-Range Weather
126 Forecasts (ECMWF) ERA5 reanalysis from 1940 to 2022. The jet latitude and strength are



127 computed by 200 hPa zonal winds over the region (50° – 80°E, 10° – 60°N). The jet latitude is the
128 mean of the latitudes with the largest value of u for each longitude and jet strength is the mean
129 value of u along these latitudes. ERA5 data have global coverage at hourly frequency and a
130 horizontal resolution of 0.25°.

131

132 **2.1.2) Precipitation data**

133 Precipitation in the KH is mainly observed through satellite derived and reanalysis products
134 (Bosilovich et al., 2008; Joshi et al., 2012; Ménégoz et al., 2013; Palazzi et al., 2013; Rana et al.,
135 2015; Kishore et al., 2016; Baudouin et al., 2020) due to limited and unreliable observations from
136 ground stations in this complex topographical region (Anders et al., 2006; Bookhagen and Burbank
137 2006; Strangeways, 2010; Rana et al., 2015; Dahri et al., 2018). The ERA5 reanalysis has
138 frequently been used for precipitation and snow in recent studies over the KH (Dahri et al., 2018;
139 Baudouin et al., 2020; T. Singh et al., 2021) and neighbouring mountainous areas (Hu and Yuan,
140 2020; Li et al. 2021; Dollan et al., 2014). ERA5 closely matches the most reliable gridded
141 measurements over KH in terms of amount, seasonality, and variability across all timescales during
142 winter (Baudouin et al., 2020). However, the accuracy of precipitation datasets varies depending on
143 the season in the region.

144 To assess the performance of ERA5 precipitation, we compared the ERA5 precipitation with
145 various gridded precipitation datasets over the KH, including reanalysis datasets from ECMWF
146 ERA5-land, Modern Era Retrospective-analysis for Research, Applications version 2 (MERRA2),
147 and High Asia Refined analysis version 2 (HAR v2), as well as rain gauge, and satellite data from
148 Climate Research Unit version 7 (CRU_TS v7), Global Precipitation Climatology Center version
149 2022 (GPCC), Global Precipitation Climatology Project version 3.2 (GPCP v3.2), Asian
150 Precipitation - Highly-Resolved Observed Data Integration Towards Evaluation (APHRODITE
151 MA_v1101), CPC-Merged Analysis of Precipitation (CMAP), Tropical Rainfall Measuring Mission
152 (TRMM) Multi-satellite Precipitation Analysis (TMPA) 3B43, and Global Precipitation
153 Measurement mission-Integrated Multi-satellite Retrievals version 7 (GPM_IMERG v7).

154 We calculated the linear correlation coefficient between area-averaged precipitation over the KH in
155 ERA5 and that in other selected datasets. A high correlation was found between DJF ERA5
156 precipitation and other precipitation products such as APHRODITE and GPCC (Table.1). All the
157 reanalysis products, including ERA5, demonstrate similar winter precipitation quantities and
158 variability as found in observations over the KH region across all timescales (Baudouin et al. 2020).



159 As all of DJF precipitation in KH is in the form of snowfall (fig. 1b), we use ERA5 snowfall data to
160 investigate the decadal variations of snowfall in the KH (73° – 78°E, 33° – 38° N).

161

162 **Table:1 Correlation coefficients of DJF precipitation based on reanalysis, rain-gauge and**
163 **satellite with ERA5 precipitation**

	Name	Time	Spatial resolution	Correlation with ERA5	Source
Reanalysis	ERA5-land	1980-2023	0.25°	0.99	Hersbach et al., 2018
	HAR v2	1980-2020	0.1°	0.97	Wang et al., 2021
	MERRA2	1980-2023	0.5°	0.92	Gelaro et al., 2017
Rain-gauge based	CRU_TS v7	1980-2023	0.5°	0.84	Harris et al., 2014
	GPCC v2022	1980-2020	2.5°	0.82	Schneider et al., 2018
	GPCP	1998-2023	2.5°	0.80	Adler et al., 2016
	CMAP	1980-2023	2.5°	0.43	Xie and Arkin, 1997
	APHRODITE	1951-2007	0.25°	0.77	Yatagai et al., 2012
Satellite	GPM_IMERG v07	2000-2023	0.1°	0.82	Huffman et al., 2015
	TRMM 3B43	1998-2019	0.25°	0.80	Huffman et al., 2007

164

165 **2.1.2) PDO index**



166 The PDO index from the National Oceanic and Atmospheric Administration National Climate Data
167 Center (NOAA-NDC) (<https://www.ncei.noaa.gov/access/monitoring/pdo/>) is employed to describe
168 the interdecadal variability of the Pacific Ocean over the period 1940 to 2022.

169

170 **2.1.3) Western disturbance data**

171 WD statistics are computed from the WD track catalogue described in Hunt et al., (2018) and
172 Nischal et al., (2022), which is based on ERA5 reanalysis data that is spectrally truncated to T42 to
173 remove noise and small-scale structures. The tracking algorithm detects WDs by identifying upper-
174 tropospheric regions of positive relative vorticity averaged between 450 hPa and 300 hPa, with the
175 locations of candidate WDs identified as centroids of these regions. The candidate WDs are then
176 further refined by only accepting those: 1) whose locations are linked through time to form tracks
177 that generally follow the westerly steering winds associated with the STJ, 2) that persist for at least
178 48 hours, and 3) that pass through north India (50° – 77° E, 22° – 42.5° N). The northern limit of this
179 box, 42.5° N, is more poleward than has been used previous studies (36.5° N). This allows us to
180 better capture WD impacts over the Karakoram.

181

182 **2.2 Methods**

183

184 **2.2.1) Lanczos filter**

185 To isolate the decadal signals, we linearly detrended all meteorological variables and the PDO index
186 for DJF. These datasets were then filtered using a 9-year running mean Lanczos filter, which is a
187 low-pass filter based on the sinc convolution (Duchon et al., 1979). The positive (negative) phase of
188 PDO is defined as years when the filtered DJF PDO index is greater than (less than) zero. We define
189 the negative epoch (PDO-) as two negative phases of PDO that occurred from 1948 to 1977 and
190 1989 to 2014, and the positive epoch (PDO+) as a positive phase of PDO that occurred from 1978
191 to 1988 (fig.1b). Also, the detrended variables are used to conduct correlation and composite
192 analyses. The Student's and Welch's t-test are used in the study to determine the statistical
193 significance of correlation and composite analyses, respectively.

194

195 **2.2.2) Wavelet analysis**



196 The PyCWT library (<https://pycwt.readthedocs.io/en/latest/tutorial/cwt/>) is used to calculate the
197 cross wavelet power spectrum. This library is based on the implementation by Torrence and Compo
198 (1998). We employed the cross wavelet transform to calculate the wavelet spectrum between
199 monthly time series of the PDO index and the area averaged monthly ERA5 snowfall over the KH
200 region. The cross wavelet transform finds regions in time frequency space where the time series
201 show high common power.

202

203

204 **3) Results:**

205 **3.1) PDO and KH winter snowfall**

206 This study aims to examine the long-term variability in DJF snowfall in the KH region in relation
207 with the PDO from 1940 to 2022. There is a significant negative correlation between the lowpass-
208 filtered and detrended time series of DJF PDO and DJF snowfall in the KH (Fig 1b), with a
209 coefficient of -0.43. However, the PDO is not a single phenomenon, but rather a set of processes
210 that occur in both the tropics and the extratropics and reflects the influence of various processes
211 occurring at distinct timescales (Newman et al., 2016). More precisely, elevated sea surface
212 temperature (SST) in the eastern tropical Pacific is linked to lower SST in the central and western
213 North Pacific, while higher SST is observed in the eastern North Pacific (Deser et al. 2004;
214 Newman et al., 2016). Thus, decadal variability of the North Pacific SST can be linked to tropical
215 Pacific decadal variability, specifically in terms of the long-lasting seasonal ENSO patterns
216 (Newman et al., 2011; Wittenberg et al. 2014). When the influence of ENSO is eliminated, the
217 correlation increases slightly to -0.45.

218

219 The spatial structure of the correlation between PDO and KH snowfall in winter (Fig 2a) is
220 significantly negative along the western and central Himalayas and much of the southern
221 Karakoram, but positive over the Tibetan Plateau and north India. The snowfall in the KH region
222 during the boreal autumn (SON) and spring (MAM) has a strong positive correlation with the PDO
223 (not shown), whereas the summer monsoon season (JJA) displays a weak but positive correlation
224 with the PDO. The different signs of the correlation suggest that the dynamic processes driving KH
225 snowfall either vary by season, or the seasonal influence of the PDO on KH snowfall changes.

226



227 Figure 2b displays the regional distribution of the difference in detrended DJF snowfall between the
228 negative and positive phases of PDO, hereafter referred to as PDO- and PDO+, respectively. The
229 difference is significantly positive in the KH area, particularly over the southern part of the
230 Karakoram region. During PDO+, DJF snowfall over KH is nearly 7% lower than the average
231 seasonal snowfall, while during PDO- it is about 6% higher. It indicates that the difference in DJF
232 snowfall in KH varies significantly depending on the phase of the PDO across several decades. DJF
233 snowfall in the KH accounts for around 80-90% of total annual snowfall during the time period (not
234 shown), hence a 15% difference in DJF snowfall can have a significant influence on agriculture in
235 this region, especially since most of the rivers in this region, such as tributaries of Indus, Tarim and
236 Ganges are partially fed by snowmelt in the spring and later seasons (Armstrong et al., 2018).

237

238 This strong relationship between PDO and snowfall in the KH is also demonstrated through a cross
239 wavelet frequency spectrum analysis between the unfiltered monthly time series of PDO index and
240 snowfall over the KH from 1940 to 2022 (Fig 2c). The band of strong and significant power in the
241 period of ~1 year in the cross-wavelet indicates that the PDO and KH snowfall both have strong
242 interannual variability. The well-known influence of ENSO on snowfall in the region (operating on
243 interannual timescales) during DJF is also slightly modulated by the low-frequency oscillation of
244 PDO. Another band of strong power lies in periods of 6-15 years which suggests a robust decadal
245 scale relationship between these two time series. The significant power in the 6-15-year range
246 occurred during the periods from 1940 to 1970 and 1998 to 2014, coinciding with the negative
247 phase of the PDO. There is an insignificant power from 1977 to 1988, which occurred during the
248 positive phase of the PDO. This suggests that the interdecadal variability of KH snowfall depends
249 on the phase of the PDO.

250

251 **3.2) Sea Surface temperature (SST) variability during DJF**

252 Figure 3a illustrates the well-known positive (or warm) phase of the PDO over the North Pacific,
253 shown as a correlation between lowpass filtered and detrended sea surface temperature (SST) and
254 PDO index during DJF. The correlation pattern also reveals a strong El-Nino like pattern in the
255 eastern equatorial-tropical Pacific Ocean. For comparison, the correlation pattern between the DJF
256 SST anomalies and the DJF snowfall anomalies in the KH region is shown in Fig 3b. This
257 correlation strongly resembles the negative (or cool) phase of the PDO over the North Pacific
258 Ocean. It is characterised by positive SST anomalies in the northwest Pacific and negative SST



259 anomalies in the northeast Pacific. Additionally, there are negative SST correlations in the tropical
260 eastern Pacific region and eastern Indian Ocean adjacent to Western Australia, while positive
261 correlations are observed in the southwest Indian Ocean and across the northwest Atlantic Ocean.
262 The correlation pattern in the southern Indian Ocean reveals the subtropical Indian Ocean Dipole
263 signature (positive phase) (Behera & Yamagata, 2001; Yamagami & Tozuka, 2014).

264

265 **3.3) Upper atmosphere circulation response with PDO and snowfall**

266

267 In order to understand the anomalous atmospheric circulations that connect the PDO with
268 anomalous DJF snowfall in the KH region, we computed the correlation of 200 hPa geopotential
269 height with both the DJF PDO index (Fig 4a) and DJF snowfall (Fig 4b). The correlation pattern
270 between the PDO and upper level geopotential height shows a prominent upper-level trough over
271 east China, Japan and the northwest Pacific, which is known as East Asian trough (EAT; Qin et al.,
272 2018; Yin and Zhang, 2021). In contrast, the correlation pattern over the Caspian Sea, KH, and Lake
273 Baikal region is associated with positive geopotential height anomalies. The EAT is a well-known
274 upper atmospheric response to the positive phase of PDO to the East Asia-North Pacific region
275 during the Northern Hemisphere winter (Newman et al, 2016; Qin et al., 2018; Yin and Zhang,
276 2021). The intensity of the EAT is strongly linked to the strength of the winter monsoon in East Asia
277 and the tilt in the EAT axis is connected to midlatitude baroclinic processes, such as the eddy-driven
278 jet or WD tracks over the East Asia-North Pacific region (Wang et al., 2009). Therefore, changes in
279 location and intensity of the EAT can lead to, or otherwise indicate, regional climate anomalies,
280 such as temperature in the upper troposphere which subsequently influence DJF precipitation in
281 East Asia as well as the KH during the positive phase of the PDO.

282 These patterns change sign during negative phases of PDO, when KH snowfall is enhanced,
283 implying an anomalous upper-level trough to the west of the Karakoram, consistent with increased
284 WD frequency or intensity. The correlation between upper-level geopotential height and snowfall
285 has a similar pattern to the PDO-geopotential correlation, but as expected, with reversed sign. The
286 correlation pattern exhibits a strong ridge (or a weakened EAT) over the northwest Pacific and
287 Japan characterised by the significant positive geopotential height anomalies. The negative
288 correlation to the west of the KH area shows a trough, which is stronger than the positive
289 correlation between PDO and geopotential height, indicating the linkage of seasonal snowfall to the
290 passage of WDs is stronger than the link between the PDO and WDs. Both, however, are important.



291 The appearance of the anomalous trough in both pairs of correlations implies that the PDO may
292 affect KH snowfall by somehow modulating WD activity. Therefore, it is essential to understand
293 how decadal fluctuations in DJF snowfall in the KH are driven by WDs and how the PDO
294 influences WD behaviour. This can be accomplished by investigating the DJF STJ, followed by a
295 detailed investigation of the WDs.

296

297 **3.4) Modulation of WD and Subtropical Westerly Jet by the PDO**

298 To further illustrate the above relationship between PDO and DJF snowfall in KH, we examine the
299 composite differences in 200 hPa wind, geopotential height, and temperature (Fig. 5) between PDO-
300 and PDO+. Figure 5a displays the difference in 200 hPa circulation over East Asia, Arabian
301 Peninsula and northwest Pacific region. During the PDO-, there is a large negative geopotential
302 height anomaly to the north of KH region, which extends from the Caspian Sea-Arabian Peninsula
303 to KH. Strong westerlies are observed to the south of this trough with a stronger STJ prevailing
304 across KH during the PDO-. An anomalous trough in the upper atmosphere is indicative of
305 increased WD frequency (or intensity) and the frequency of WDs is strongly affected by variations
306 in both the latitude and intensity of the STJ (Dimri et al., 2015; Hunt et al., 2017, 2018) over South
307 Asia. Therefore we now focus on understanding the relationship between the PDO and the STJ.

308

309 Upper-level jets are thermal wind responses to upper-level meridional temperature gradients. In Fig
310 5b, we show the difference in mid-to-upper (from 500 hPa to 300 hPa) tropospheric temperature
311 between PDO- and PDO+. A quadrupole in the upper air temperature gradient is present across the
312 KH, Tibetan Plateau (TP) and the northwest Pacific region during PDO-. Over the Pacific, this is
313 effectively a direct response to the anomalous surface heating provided by the PDO. Anomalous
314 warm SSTs over the northwest Pacific lead to adiabatic cooling near the tropopause, which results
315 in deep convection over the Maritime Continent during the PDO- (e.g., Wang et al., 2016).
316 Upstream, over continental Asia, the relationship is more complicated and is probably a wave
317 response to the direct forcing over the ocean. Therefore, a strongly enhanced meridional
318 temperature gradient over the KH and TP, leading to a stronger and more meridionally-locked STJ.

319

320 Figure 5c displays the lowpass filtered time series of latitude and strength of the DJF STJ. During
321 the PDO-, the STJ tends to sit slightly further north but is also substantially stronger. The



322 correlation of the time series of the strength of DJF STJ with DJF PDO is significantly negative (-
323 0.22), and the correlation between DJF STJ strength and DJF snowfall in KH significantly positive
324 (0.36). The positive (negative) phase of the PDO enhances the movement of the STJ towards the
325 south (north) through a response to the decreased (increased) SST over the northwest Pacific and
326 modulates the cyclonic (anticyclonic) circulation over the northwest Pacific and adjacent maritime
327 continents (Matsumura & Horinouchi, 2016). During PDO-, we observed a quadrupole in the
328 anomalous upper level temperature gradient (Fig. 5b), resulting in a negative anomaly in the
329 temperature gradient and an anticyclonic circulation (Fig. 5a) over the TP. Thus, by modulating the
330 STJ, the negative phase of the PDO leads to more frequent (more intense) WDs at slightly higher
331 latitudes than usual (e.g. into the Karakoram, where the signal is the strongest).

332

333 The presence of a stronger STJ along with a wave-like pattern of trough (anomalous cyclone) over
334 the northern region of KH, and a ridge (anomalous TP anticyclone) in the upper atmosphere,
335 increases the occurrence of WDs over KH during the PDO-. After examining the impact of the PDO
336 on the STJ, we now quantify its influence on WDs directly. Maps of the difference in the frequency
337 of DJF WDs between PDO- and PDO+ (Fig 6a) indicate that WDs are more frequent (with a 9%
338 higher frequency) over the KH region during PDO- compared to PDO+. Also, the frequency of
339 WDs is found to be reduced by around 3% in both the northern and southern regions of the KH
340 during PDO- compared to PDO+. These WDs are observed to be more intense in the vicinity of the
341 Caspian Sea and north of the KH during PDO- rather than PDO+ (not shown).

342

343 **3.5) Atmospheric-ocean response of PDO on moisture transport in KH**

344 Increased frequency and intensity of WDs have a significant impact on precipitation in the KH and
345 surrounding region because they govern southwesterly moisture transport from the Arabian Sea
346 (Baudouin et al., 2021; Hunt and Dimri 2021). The composite difference of DJF VIMF and VIMFC
347 between PDO- and PDO+ is now examined to determine the response of moisture transport to the
348 PDO and its subsequent effect on the KH (Fig. 6b)

349 The average difference of VIMFC between PDO- and PDO+ is about $0.8 \times 10^{-5} \text{ kg m}^{-2} \text{ s}^{-1}$ within
350 KH region. An advection of moisture from the Black Sea, Red Sea, and eastern Mediterranean Sea
351 through the Arabian Peninsula/Arabian Sea towards the KH in westerly fashion is observed. The
352 precipitation associated with WDs is mostly determined by their intensity and proximity to the
353 Arabian Sea (Baudouin et al., 2020). The variations in the moisture transport across the Arabian



354 Peninsula/Arabian Sea are not directly linked to changes in VIMF over the northwest Pacific, but
355 the presence of more WDs south of the strong DJF STJ over KH clearly result in greater moisture
356 transport towards KH during PDO-. Hence, the anomalous moisture transport nearly perpendicular
357 to KH, results in increased moisture flux convergence and consequently greater precipitation in the
358 region during PDO-.

359

360 **4) Conclusion and Discussion:**

361 The recent impacts of climate change over the KH, particularly in mean and extreme winter
362 precipitation, have been largely attributed largely to anthropogenic forcing, such as greenhouse
363 gases, aerosols, and changes in land use. However, these changes cannot be solely explained by
364 natural forcing (Krishnan et al., 2018). Oceanic conditions, especially changes in SSTs over the
365 equatorial-tropical Pacific and north Pacific, play an important role in driving interdecadal
366 variability in atmospheric circulation and hence winter precipitation over the KH .

367 Understanding this interdecadal variability and its relationship with the PDO is important for
368 understanding the long-term climate of the KH. We have analysed the long-term variability in
369 winter snowfall over the KH due to the PDO by using ERA5 reanalysis data from 1940 to 2022. We
370 found that a strong negative correlation of -0.43 between the PDO and DJF snowfall in the KH.
371 Mean KH snowfall during DJF is approximately 6% greater than the DJF seasonal average during
372 PDO-, and 7% lower during PDO+.

373

374 PDO associated anomalous warming of SST in the northwest Pacific modulates the snowfall in the
375 KH via changes in upper-level temperatures over the Pacific and Asia. The warm SSTs lead to
376 increased deep convection and subsequent upper-tropospheric adiabatic cooling over the Pacific.
377 During PDO-, the anomalous heating of the tropospheric column over North Pacific leads to a wave
378 like pattern with an upper-level trough over the north of KH and upper-level ridge over the Tibetan
379 Plateau. This results in a stronger STJ to the west of, and over, the KH, before it is deflected
380 northwards over the Tibetan Plateau. There is a strong positive correlation between the strength of
381 DJF STJ and DJF snowfall in KH, with a correlation coefficient of 0.36, and a significant negative
382 correlation between the strength of STJ and PDO, with a correlation coefficient of -0.22 during DJF
383 at decadal scale. These results suggest a wave response over KH to the direct forcing over the
384 Pacific Ocean.



385 These anomalous jet conditions over KH are linked to a higher occurrence of WDs across the
386 region. Using a track catalogue, we found that WDs are 9% more frequent across the KH and drop
387 by approximately 3% in both the northern and southern regions of the KH during PDO- compared
388 to PDO+. However, the WDs are found to be more intense in the vicinity of the Caspian Sea and
389 north of the KH during PDO- rather than PDO+, which is not shown in this study. This increase in
390 WD frequency results in anomalous moisture transport from the Arabian Sea, Black Sea, Red Sea,
391 and eastern Mediterranean Sea towards the KH. The moisture transport is almost perpendicular to
392 the orography of the KH, leading to a strong moisture convergence and thus increased DJF
393 precipitation in the region during the negative phases of the PDO.

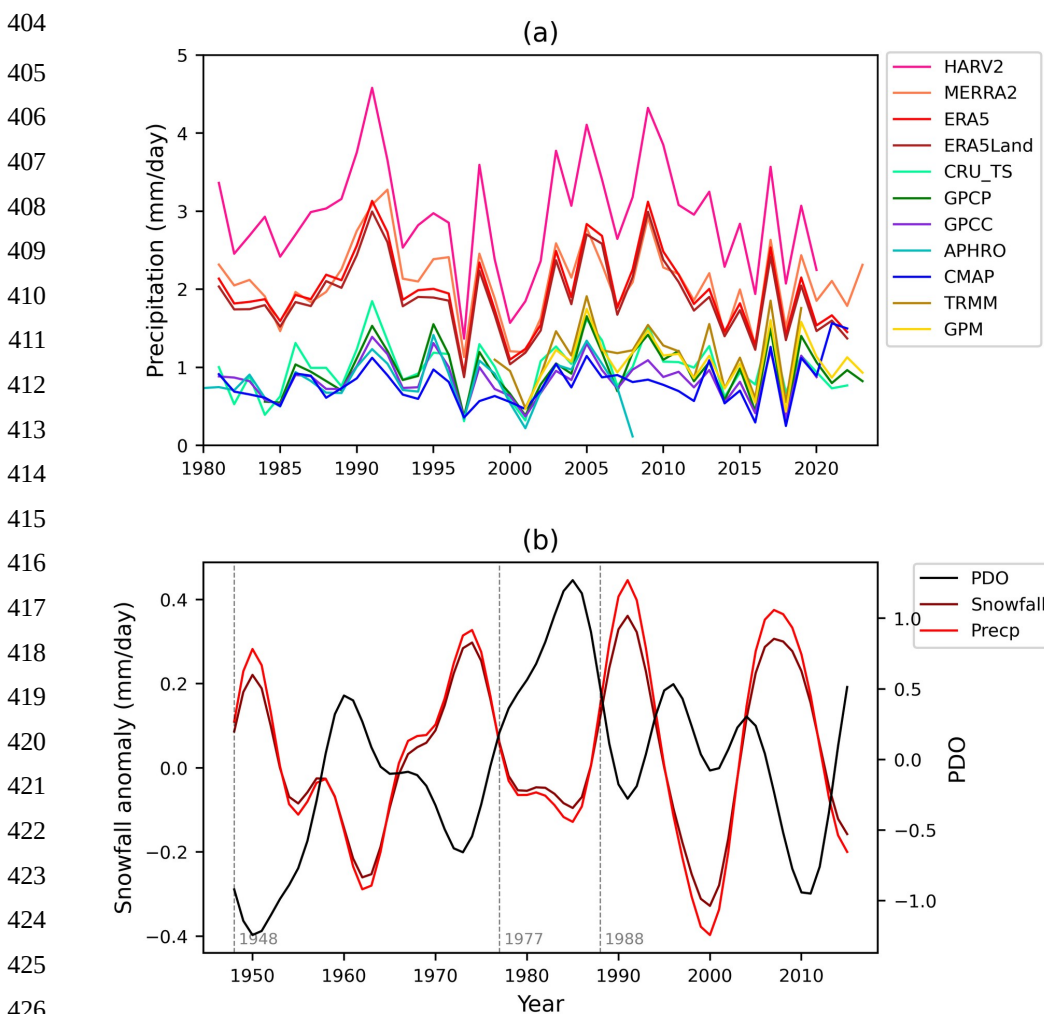
394 Our findings highlight the importance of considering interdecadal variability when trying to
395 quantify the effects of anthropogenic climate change in the KH. The recent PDO- has led to
396 increased WD activity, and hence increased winter snowfall over this region, and may be masking
397 the effects of climate change. More research is needed to disentangle climate change from the
398 effects of interdecadal variability over this vulnerable region, so that policymakers can be better
399 informed.

400

401 **5) List of figures:**

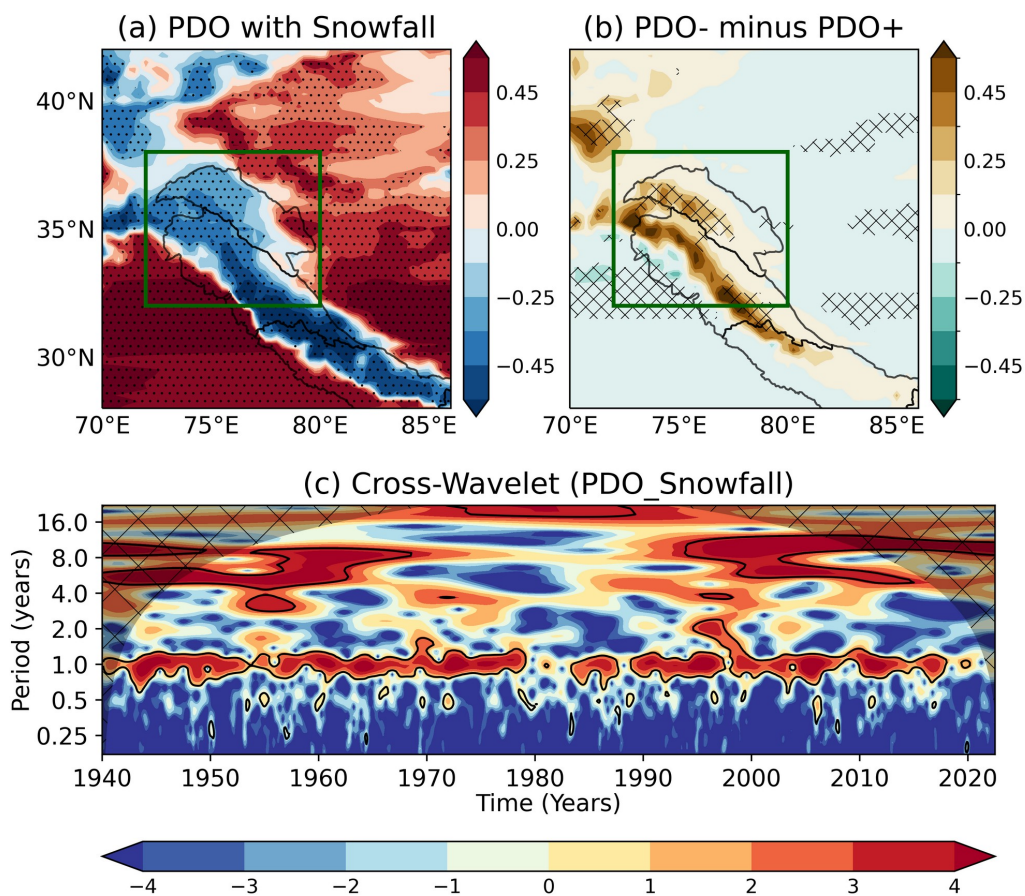
402

403



427 **Figure 1: (a) Seasonal variability of DJF precipitation in KH (green rectangle in fig.2; 73-78E,**
428 **33-38N) from ERA5, ERA5-land, MERRA2, HARv2, CRU_TS, GPCP, GPCP, and CMAP**
429 **during the period from 1980 to 2020, APHRODITE from 1951 to 2007, TRMM from 1998 to**
430 **2019, and GPM from 2000 to 2023. (b) Time series of 9-year filtered DJF PDO index and area-**
431 **averaged DJF ERA5 snowfall (and precipitation) anomalies over KH from 1940 to 2022. The**
432 **vertical grey lines represent phase transitions of PDO.**

433



435
436 **Figure 2: (a) Spatial map of correlation between the 9-year filtered PDO index and the**
437 **snowfall over KH during DJF, and (b) composite difference of DJF snowfall between negative**
438 **and positive epoch of PDO, (c) cross-wavelet of DJF snowfall over KH and DJF PDO index**
439 **from 1940 to 2022. Stippling in (a) and (b) indicate where the correlation, composite**
440 **differences are significant at a 95% confidence level. Black line contours on the power spectra**
441 **in (c) indicate where the spectral power of the cross-wavelet is significantly greater than zero**
442 **at a 95% confidence level.**

443

444

445

446

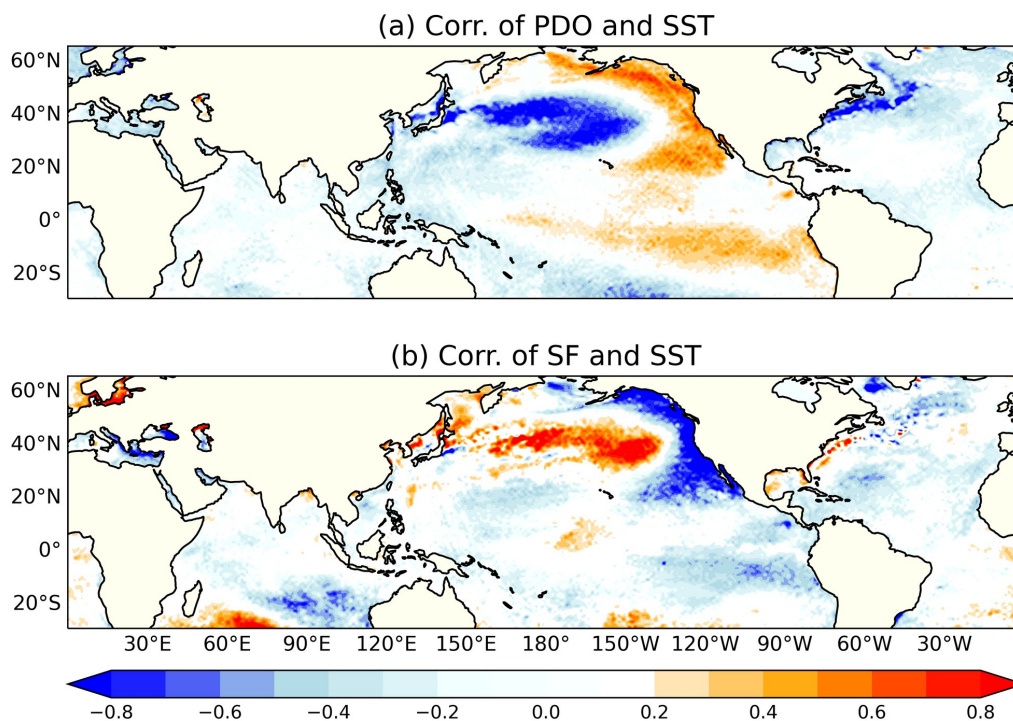


447

448

449

450



451 **Figure 3: Spatial map of correlation of the 9-year filtered (a) DJF PDO index, and (b) area**
452 **averaged DJF snowfall over the green box (fig.2) with 9-year filtered DJF sea surface**
453 **temperature from 1940 to 2022. The correlations are significant at a 95% confidence level.**

454

455

456

457

458

459

460

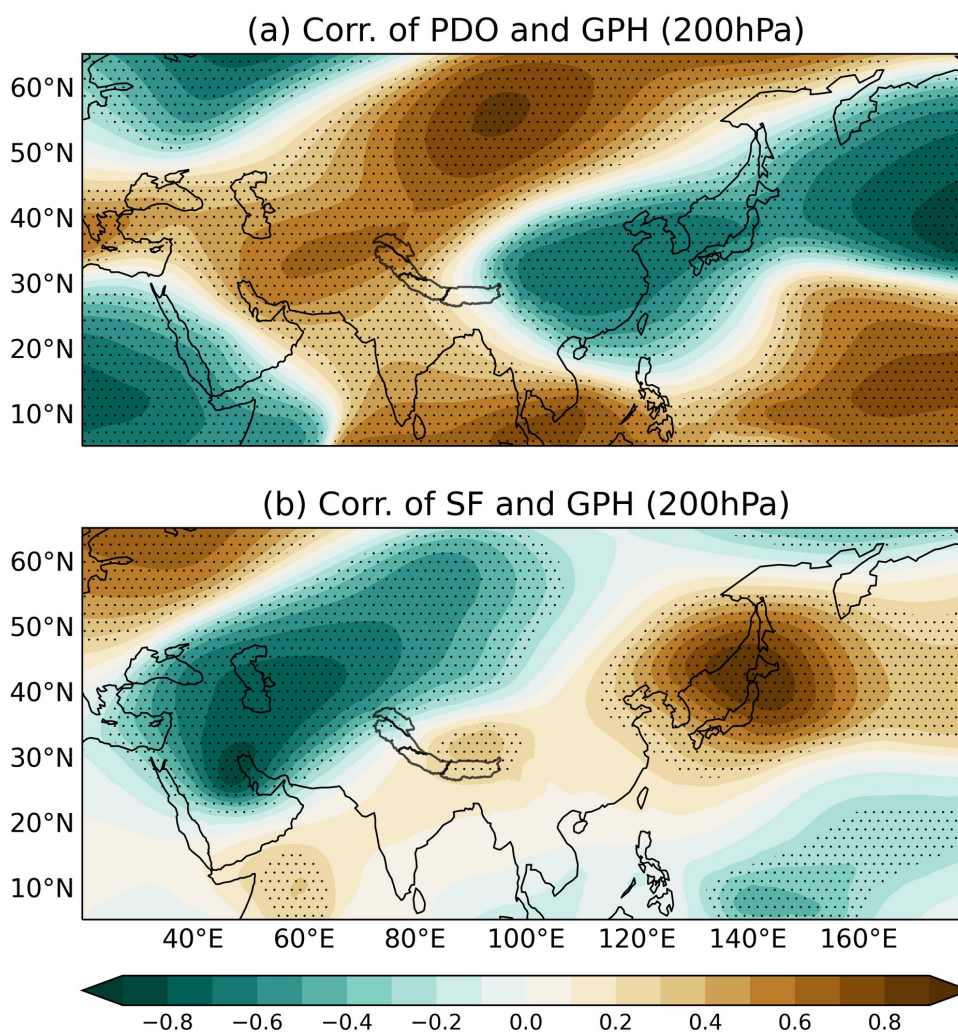
461



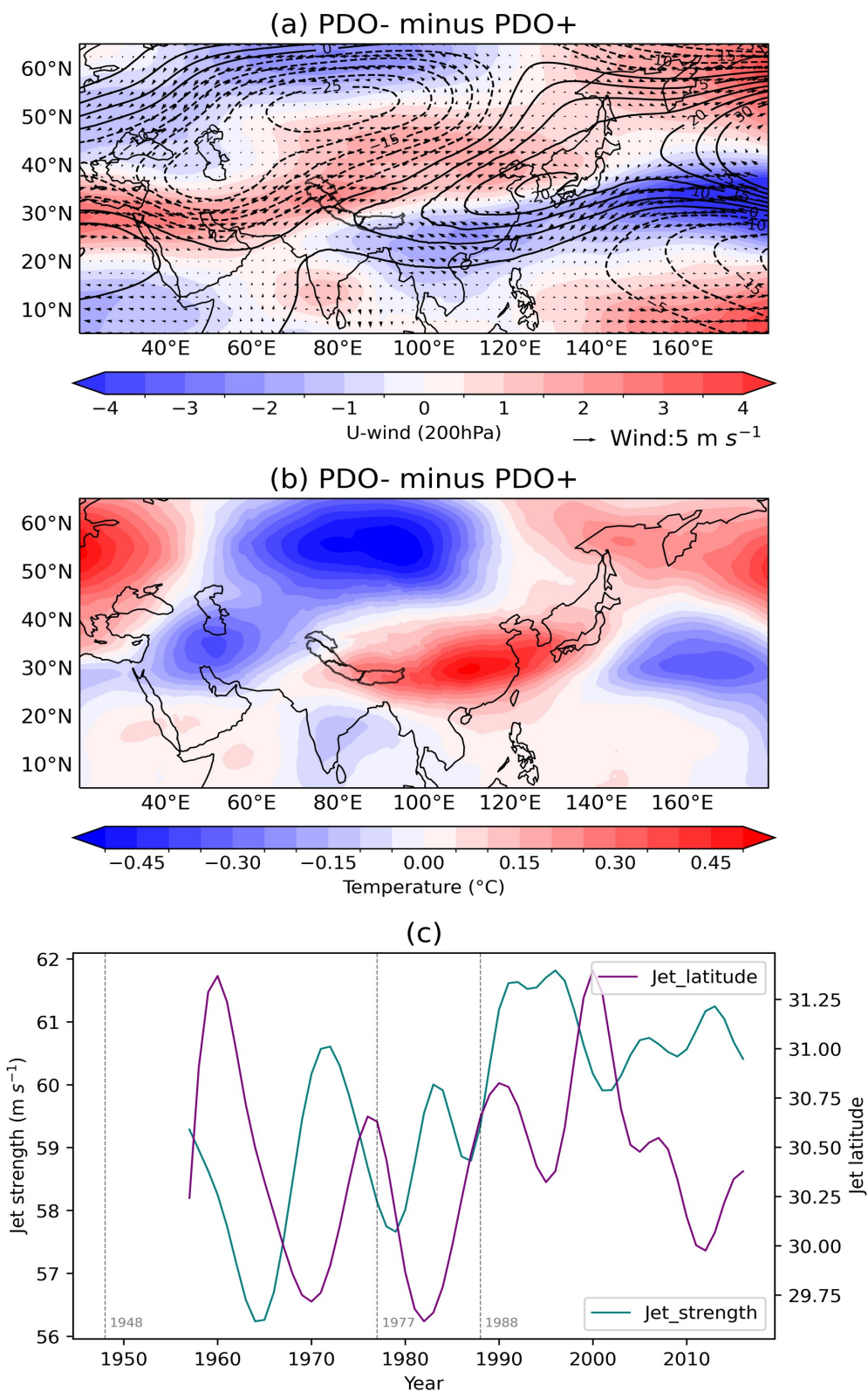
462

463

464



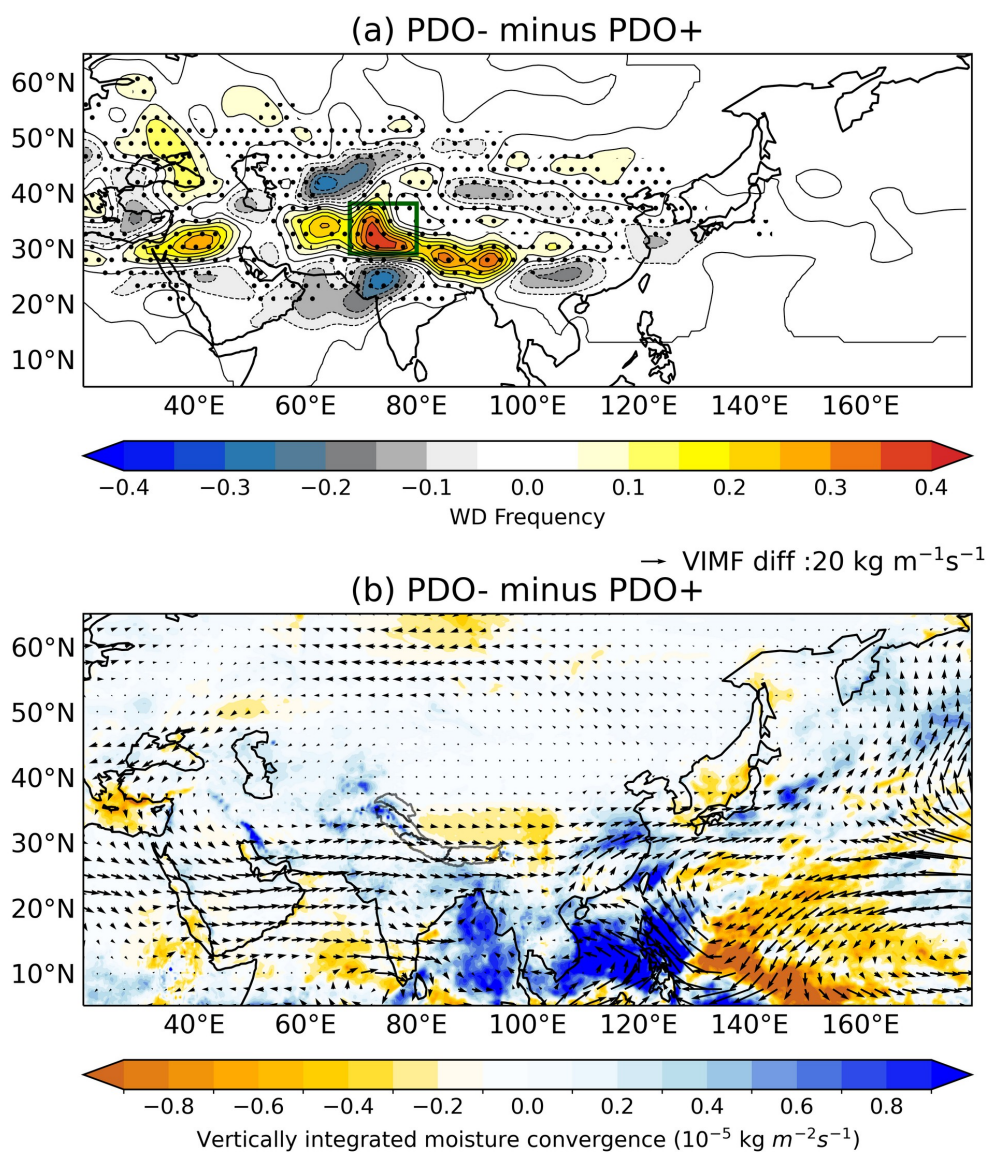
466 **Figure 4: Spatial map of correlation of the 9-year filtered (a) DJF PDO index, and (b) area**
467 **averaged DJF snowfall over the green box (fig.2) with 9-year filtered DJF geopotential height**
468 **at 200hPa (m) from 1940 to 2022. Stipplings in (a) and (b) indicate where the correlations are**
469 **significant at a 95% confidence level.**





471 **Figure 5: Composite difference of (a) U-wind (colour; m/s), wind (vectors; m/s), and**
472 **geopotential height (contours; m), (b) vertically averaged temperature (C) from 300hPa to**
473 **500hPa level during DJF between negative and positive epoch of PDO, (c) time series of 9-year**
474 **filtered strength (red) and latitude (blue) of DJF subtropical westerly jet (STJ) over KH**
475 **(green box; fig.2) from 1940 to 2022.**

476
477



478 **Figure 6: Composite difference of (a) WD frequency, and (b) vertically integrated moisture**
479 **flux (vectors; kg/m/s) and vertically integrated moisture convergence (colours; kg/m²/s)**



480 **during DJF between negative and positive epoch of PDO from 1940 to 2022. Stippling in (a)**
481 **indicates where the differences are significant at a 95% confidence level.**

482

483 **Author Contributions:**

484 **Priya Bharati:** conceptualization; formal analysis; methodology; investigation; software;
485 visualization; writing original draft. **Kieran M. R. Hunt:** conceptualization; methodology;
486 software; writing - review and editing. **Pranab Deb:** supervision; conceptualization; writing –
487 review and editing.

488

489 **Competing interests:** The contact author has declared that none of the authors has any
490 competing interests.

491 **Acknowledgements:**

492 The work is carried at CORAL, Indian Institute of Technology Kharagpur under supervision of
493 Pranab Deb. Priya Bharati is funded through the Ministry of Science and Technology, Government
494 of India, Council of Scientific and Industrial Research (CSIR; 09/081(1371)/2019-EMR-I). KMRH
495 is supported by a NERC Independent Research Fellowship (MITRE; NE/W007924/1).

496

497 **References:**

498 Adler, R., Sapiano, M., Huffman, G., Bolvin, D., Gu, G., Wang, J., Nelkin, E., Xie, P., Chiu, L.,
499 Ferraro, R. and Schneider, U., 2016. The new version 2.3 of the Global Precipitation Climatology
500 Project (GPCP) monthly analysis product. University of Maryland, April, pp.1072-1084.

501

502 Archer, D.R. and Fowler, H.J., 2004. Spatial and temporal variations in precipitation in the Upper
503 Indus Basin, global teleconnections and hydrological implications. *Hydrology and Earth System*
504 *Sciences*, 8(1), pp.47-61.

505

506 Armstrong, R.L., Rittger, K., Brodzik, M.J., Racoviteanu, A., Barrett, A.P., Khalsa, S.J.S., Raup, B.,
507 Hill, A.F., Khan, A.L., Wilson, A.M. and Kayastha, R.B., 2019. Runoff from glacier ice and



508 seasonal snow in High Asia: separating melt water sources in river flow. *Regional Environmental*
509 *Change*, 19, pp.1249-1261.

510

511 Barlow, M., Wheeler, M., Lyon, B. and Cullen, H., 2005. Modulation of daily precipitation over
512 southwest Asia by the Madden–Julian oscillation. *Monthly weather review*, 133 (12), pp.3579-3594.

513

514 Basu, S., Bieniek, P.A. and Deoras, A., 2017. An investigation of reduced western disturbance
515 activity over Northwest India in November–December 2015 compared to 2014–A case study. *Asia-*
516 *Pacific Journal of Atmospheric Sciences*, 53, pp.75-83.

517

518 Baudouin, J.P., Herzog, M. and Petrie, C.A., 2020. Cross-validating precipitation datasets in the
519 Indus River basin. *Hydrology and Earth System Sciences*, 24(1), pp.427-450.

520

521 Beck, H.E., Pan, M., Roy, T., Weedon, G.P., Pappenberger, F., Van Dijk, A.I., Huffman, G.J., Adler,
522 R.F. and Wood, E.F., 2019. Daily evaluation of 26 precipitation datasets using Stage-IV gauge-radar
523 data for the CONUS. *Hydrology and Earth System Sciences*, 23(1), pp.207-224.

524

525 Behera, S.K. and Yamagata, T., 2001. Subtropical SST dipole events in the southern Indian Ocean.
526 *Geophysical Research Letters*, 28(2), pp.327-330.

527

528 Bolch, T., Kulkarni, A., Kääb, A., Huggel, C., Paul, F., Cogley, J.G., Frey, H., Kargel, J.S., Fujita,
529 K., Scheel, M. and Bajracharya, S., 2012. The state and fate of Himalayan glaciers. *Science*,
530 336(6079), pp.310-314.

531

532 Bonekamp, P.N., De Kok, R.J., Collier, E. and Immerzeel, W.W., 2019. Contrasting meteorological
533 drivers of the glacier mass balance between the Karakoram and central Himalaya. *Frontiers in Earth*
534 *Science*, 7, p.107.

535



536 Bookhagen, B. and Burbank, D.W., 2010. Toward a complete Himalayan hydrological budget:
537 Spatiotemporal distribution of snowmelt and rainfall and their impact on river discharge. *Journal of*
538 *Geophysical Research: Earth Surface*, 115(F3).

539

540 Bosilovich, M.G., Chen, J., Robertson, F.R. and Adler, R.F., 2008. Evaluation of global
541 precipitation in reanalyses. *Journal of applied meteorology and climatology*, 47(9), pp.2279-2299.

542

543 Cannon, F., Carvalho, L.M., Jones, C. and Bookhagen, B., 2015. Multi-annual variations in winter
544 westerly disturbance activity affecting the Himalaya. *Climate dynamics*, 44, pp.441-455.

545

546 Cannon, F., Carvalho, L.M., Jones, C., Hoell, A., Norris, J., Kiladis, G.N. and Tahir, A.A., 2017.
547 The influence of tropical forcing on extreme winter precipitation in the western Himalaya. *Climate*
548 *Dynamics*, 48, pp.1213-1232.

549

550 Dahri, Z.H., Moors, E., Ludwig, F., Ahmad, S., Khan, A., Ali, I. and Kabat, P., 2018. Adjustment of
551 measurement errors to reconcile precipitation distribution in the high-altitude Indus basin.
552 *International Journal of Climatology*, 38(10), pp.3842-3860.

553

554 de Kok, R.J., Tuinenburg, O.A., Bonekamp, P.N. and Immerzeel, W.W., 2018. Irrigation as a
555 potential driver for anomalous glacier behavior in High Mountain Asia. *Geophysical research*
556 *letters*, 45(4), pp.2047-2054.

557

558 Dimri, A.P., Niyogi, D., Barros, A.P., Ridley, J., Mohanty, U.C., Yasunari, T. and Sikka, D.R., 2015.
559 Western disturbances: a review. *Reviews of Geophysics*, 53(2), pp.225-246.

560 Dimri, A.P. and Dash, S.K., 2012. Wintertime climatic trends in the western Himalayas. *Climatic*
561 *change*, 111, pp.775-800.

562



563 Dimri, A.P. and Niyogi, D., 2013. Regional climate model application at subgrid scale on Indian
564 winter monsoon over the western Himalayas. *International Journal of Climatology*, 33(9), pp.2185-
565 2205.

566

567 Dimri, A.P., 2013. Relationship between ENSO phases with Northwest India winter precipitation.
568 *International journal of climatology*, 33(8), pp.1917-1923.

569

570 Dollan, I.J., Maina, F.Z., Kumar, S.V., Nikolopoulos, E.I. and Maggioni, V., 2024. An assessment of
571 gridded precipitation products over High Mountain Asia. *Journal of Hydrology: Regional Studies*,
572 52, p.101675.

573

574 Duchon, C.E., 1979. Lanczos filtering in one and two dimensions. *Journal of Applied Meteorology*
575 *and Climatology*, 18(8), pp.1016-1022.

576

577 Dai, A., 2013. The influence of the inter-decadal Pacific oscillation on US precipitation during
578 1923–2010. *Climate dynamics*, 41(3), pp.633-646.

579

580 Deser, C., Phillips, A.S. and Hurrell, J.W., 2004. Pacific interdecadal climate variability: Linkages
581 between the tropics and the North Pacific during boreal winter since 1900. *Journal of Climate*,
582 17(16), pp.3109-3124.

583

584 Dong, B. and Dai, A., 2015. The influence of the interdecadal Pacific oscillation on temperature and
585 precipitation over the globe. *Climate dynamics*, 45, pp.2667-2681.

586

587 Enfield, D.B., Mestas-Nuñez, A.M. and Trimble, P.J., 2001. The Atlantic multidecadal oscillation
588 and its relation to rainfall and river flows in the continental US. *Geophysical research letters*,
589 28(10), pp.2077-2080.

590



591 Farinotti, D., Immerzeel, W.W., de Kok, R.J., Quincey, D.J. and Dehecq, A., 2020. Manifestations
592 and mechanisms of the Karakoram glacier Anomaly. *Nature geoscience*, 13(1), pp.8-16.

593

594 Filippi, L., Palazzi, E., von Hardenberg, J. and Provenzale, A., 2014. Multidecadal variations in the
595 relationship between the NAO and winter precipitation in the Hindu Kush–Karakoram. *Journal of*
596 *climate*, 27(20), pp.7890-7902.

597

598 Forsythe, N., Fowler, H.J., Li, X.F., Blenkinsop, S. and Pritchard, D., 2017. Karakoram temperature
599 and glacial melt driven by regional atmospheric circulation variability. *Nature Climate Change*,
600 7(9), pp.664-670.

601

602 Fowler, H.J. and Archer, D.R., 2006. Conflicting signals of climatic change in the Upper Indus
603 Basin. *Journal of climate*, 19(17), pp.4276-4293.

604

605 Gardelle, J., Berthier, E. and Arnaud, Y., 2012. Slight mass gain of Karakoram glaciers in the early
606 twenty-first century. *Nature geoscience*, 5(5), pp.322-325.

607

608 Gelaro, R., McCarty, W., Suárez, M.J., Todling, R., Molod, A., Takacs, L., Randles, C.A.,
609 Darmenov, A., Bosilovich, M.G., Reichle, R. and Wargan, K., 2017. The modern-era retrospective
610 analysis for research and applications, version 2 (MERRA-2). *Journal of climate*, 30(14), pp.5419-
611 5454.

612

613 Harris, I.P.D.J., Jones, P.D., Osborn, T.J. and Lister, D.H., 2014. Updated high-resolution grids of
614 monthly climatic observations—the CRU TS3. 10 Dataset. *International journal of climatology*,
615 34(3), pp.623-642.

616

617 Hersbach, H., de Rosnay, P., Bell, B., Schepers, D., Simmons, A., Soci, C., Abdalla, S., Alonso-
618 Balmaseda, M., Balsamo, G., Bechtold, P. and Berrisford, P., 2018. Operational global reanalysis:
619 progress, future directions and synergies with NWP.



620

621 Hewitt, K., 2005. The Karakoram anomaly? Glacier expansion and the 'elevation effect', Karakoram
622 Himalaya. *Mountain Research and Development*, pp.332-340.

623

624 Hewitt, K., 2014. Glaciers of the Karakoram Himalaya. *Encyclopedia of Snow, Ice and Glaciers*,
625 edited by: Singh, VP, Singh, P., and Haritashya, UK, Springer Netherlands, Dordrecht, pp.429-436.

626

627 HIMAP, 2020. In: Wester, Philippus, Mishra, Arabinda, Mukherji, Aditi, Shrestha, Arun Bhakta
628 (Eds.), *The Hindu Kush Himalaya Assessment: Mountains, Climate Change, Sustainability and*
629 *People*. Springer.

630

631 Hoell, A., Barlow, M. and Saini, R., 2013. Intraseasonal and seasonal-to-interannual Indian Ocean
632 convection and hemispheric teleconnections. *Journal of Climate*, 26(22), pp.8850-8867.

633 Huffman, G.J., Bolvin, D.T., Nelkin, E.J., Wolff, D.B., Adler, R.F., Gu, G., Hong, Y., Bowman, K.P.
634 and Stocker, E.F., 2007. The TRMM multisatellite precipitation analysis (TMPA): Quasi-global,
635 multiyear, combined-sensor precipitation estimates at fine scales. *Journal of hydrometeorology*,
636 8(1), pp.38-55.

637

638 Huffman, G.J., Bolvin, D.T., Braithwaite, D., Hsu, K., Joyce, R., Xie, P. and Yoo, S.H., 2015.
639 NASA global precipitation measurement (GPM) integrated multi-satellite retrievals for GPM
640 (IMERG). Algorithm theoretical basis document (ATBD) version, 4(26), p.30.

641

642 Hunt, K.M., Turner, A.G. and Shaffrey, L.C., 2018. The evolution, seasonality and impacts of
643 western disturbances. *Quarterly Journal of the Royal Meteorological Society*, 144(710), pp.278-290.

644

645 Hunt, K.M. and Fletcher, J.K., 2019. The relationship between Indian monsoon rainfall and low-
646 pressure systems. *Climate Dynamics*, 53(3), pp.1859-1871.

647



648 Hunt, K.M. and Zaz, S.N., 2023. Linking the North Atlantic Oscillation to winter precipitation over
649 the Western Himalaya through disturbances of the subtropical jet. *Climate Dynamics*, 60(7),
650 pp.2389-2403.

651

652 Hu, X. and Yuan, W., 2021. Evaluation of ERA5 precipitation over the eastern periphery of the
653 Tibetan plateau from the perspective of regional rainfall events. *International Journal of*
654 *Climatology*, 41(4), pp.2625-2637.

655

656 Hunt, K. M. R., Baudouin, J.-P., Turner, A. G., Dimri, A. P., Jeelani, G., Pooja, Chattopadhyay, R.,
657 Cannon, F., Arulalan, T., Shekhar, M. S., Sabin, T. P., and Palazzi, E.: Western disturbances and
658 climate variability: a review of recent developments, *EGUsphere* [preprint],
659 <https://doi.org/10.5194/egusphere-2024-820>, 2024.

660

661 Javed, A., Kumar, P., Hodges, K.I., Sein, D.V., Dubey, A.K. and Tiwari, G., 2022. Does the recent
662 revival of western disturbances govern the Karakoram anomaly?. *Journal of Climate*, 35(13),
663 pp.4383-4402.

664

665 Joshi, M.K., Rai, A. and Pandey, A.C., 2013. Validation of TMPA and GPCP 1DD against the
666 ground truth rain-gauge data for Indian region. *International journal of climatology*, 33(12),
667 pp.2633-2648.

668

669 Kääb, A., Berthier, E., Nuth, C., Gardelle, J. and Arnaud, Y., 2012. Contrasting patterns of early
670 twenty-first-century glacier mass change in the Himalayas. *Nature*, 488(7412), pp.495-498.

671

672 Kamil, S., Almazroui, M., Kang, I.S., Hanif, M., Kucharski, F., Abid, M.A. and Saeed, F., 2019.
673 Long-term ENSO relationship to precipitation and storm frequency over western Himalaya–
674 Karakoram–Hindukush region during the winter season. *Climate Dynamics*, 53, pp.5265-5278.

675



676 Kapnick, S.B., Delworth, T.L., Ashfaq, M., Malyshev, S. and Milly, P.C., 2014. Snowfall less
677 sensitive to warming in Karakoram than in Himalayas due to a unique seasonal cycle. *Nature*
678 *Geoscience*, 7(11), pp.834-840.

679

680 Kar, S.C. and Rana, S., 2014. Interannual variability of winter precipitation over northwest India
681 and adjoining region: impact of global forcings. *Theoretical and applied climatology*, 116, pp.609-
682 623.

683

684 Kishore, P., Jyothi, S., Basha, G., Rao, S.V.B., Rajeevan, M., Velicogna, I. and Sutterley, T.C., 2016.
685 Precipitation climatology over India: validation with observations and reanalysis datasets and
686 spatial trends. *Climate dynamics*, 46, pp.541-556.

687

688 Krishnan, R., Sabin, T.P., Madhura, R.K., Vellore, R.K., Mujumdar, M., Sanjay, J., Nayak, S. and
689 Rajeevan, M., 2019. Non-monsoonal precipitation response over the Western Himalayas to climate
690 change. *Climate Dynamics*, 52, pp.4091-4109.

691

692 Krishnan, R. and Sugi, M., 2003. Pacific decadal oscillation and variability of the Indian summer
693 monsoon rainfall. *Climate Dynamics*, 21, pp.233-242.

694

695 Krishnan, R. and Sugi, M., 2003. Pacific decadal oscillation and variability of the Indian summer
696 monsoon rainfall. *Climate Dynamics*, 21, pp.233-242.

697

698 Krishnamurthy, L. and Krishnamurthy, V.J.C.D., 2013. Influence of PDO on South Asian summer
699 monsoon and monsoon-ENSO relation. *Climate dynamics*, 42, pp.2397-2410.

700

701 Krishnamurthy, L. and Krishnamurthy, V., 2014. Decadal scale oscillations and trend in the Indian
702 monsoon rainfall. *Climate dynamics*, 43, pp.319-331.

703



704 Lang, T.J. and Barros, A.P., 2004. Winter storms in the central Himalayas. *Journal of the*
705 *Meteorological Society of Japan. Ser. II*, 82(3), pp.829-844.

706

707 Mantua, N.J., Hare, S.R. and Zhang, Y., 1998. A Pacific interdecadal climate oscillation with
708 impacts on salmon production. *Oceanographic Literature Review*, 1(45), p.36.

709

710 Ménégoz, M., Gallée, H. and Jacobi, H.W., 2013. Precipitation and snow cover in the Himalaya:
711 from reanalysis to regional climate simulations. *Hydrology and Earth System Sciences*, 17(10),
712 pp.3921-3936.

713

714 Midhuna, T.M. and Dimri, A.P., 2019. Impact of arctic oscillation on Indian winter monsoon.
715 *Meteorology and Atmospheric Physics*, 131, pp.1157-1167.

716

717 Midhuna, T.M., Kumar, P. and Dimri, A.P., 2020. A new Western Disturbance Index for the Indian
718 winter monsoon. *Journal of Earth System Science*, 129, pp.1-14.

719

720 Newman, M., Shin, S.I. and Alexander, M.A., 2011. Natural variation in ENSO flavors.
721 *Geophysical Research Letters*, 38(14).

722

723 Newman, M., Alexander, M.A., Ault, T.R., Cobb, K.M., Deser, C., Di Lorenzo, E., Mantua, N.J.,
724 Miller, A.J., Minobe, S., Nakamura, H. and Schneider, N., 2016. The Pacific decadal oscillation,
725 revisited. *Journal of Climate*, 29(12), pp.4399-4427.

726

727 Nischal, Attada, R. and Hunt, K.M., 2022. Evaluating winter precipitation over the western
728 Himalayas in a high-resolution Indian regional reanalysis using multisource climate datasets.
729 *Journal of Applied Meteorology and Climatology*, 61(11), pp.1613-1633.

730



731 Norris, J., Carvalho, L.M., Jones, C. and Cannon, F., 2015. WRF simulations of two extreme
732 snowfall events associated with contrasting extratropical cyclones over the western and central
733 Himalaya. *Journal of Geophysical Research: Atmospheres*, 120(8), pp.3114-3138.

734

735 Norris, J., Carvalho, L.M., Jones, C., Cannon, F., Bookhagen, B., Palazzi, E. and Tahir, A.A., 2017.
736 The spatiotemporal variability of precipitation over the Himalaya: evaluation of one-year WRF
737 model simulation. *Climate Dynamics*, 49, pp.2179-2204.

738

739 Norris, J., Carvalho, L.M., Jones, C. and Cannon, F., 2019. Deciphering the contrasting climatic
740 trends between the central Himalaya and Karakoram with 36 years of WRF simulations. *Climate*
741 *Dynamics*, 52, pp.159-180.

742

743 Palazzi, E., Von Hardenberg, J. and Provenzale, A., 2013. Precipitation in the Hindu-Kush
744 Karakoram Himalaya: observations and future scenarios. *Journal of Geophysical Research:*
745 *Atmospheres*, 118(1), pp.85-100.

746

747 Power, S., Casey, T., Folland, C., Colman, A. and Mehta, V., 1999. Inter-decadal modulation of the
748 impact of ENSO on Australia. *Climate dynamics*, 15, pp.319-324.

749

750 Priya Bharati, M. R. Hunt Kieran, Mihir Kumar Dash, Pranab Deb, Andrew Orr ENSO-induced
751 latitudinal variation of the subtropical jet modulates extreme winter precipitation over the Western
752 Himalaya. doi: 10.1007/s00376-024-4057-2.

753

754 Pritchard, H.D., 2019. Asia's shrinking glaciers protect large populations from drought stress.
755 *Nature*, 569(7758), pp.649-654.

756

757 Qin, M., Li, D., Dai, A., Hua, W. and Ma, H., 2018. The influence of the Pacific Decadal Oscillation
758 on North Central China precipitation during boreal autumn. *International Journal of Climatology*,
759 38, pp.e821-e831.



760

761 Rana, S., McGregor, J. and Renwick, J., 2015. Precipitation seasonality over the Indian
762 subcontinent: An evaluation of gauge, reanalyses, and satellite retrievals. *Journal of*
763 *Hydrometeorology*, 16(2), pp.631-651.

764

765 Rana, S., McGregor, J. and Renwick, J., 2019. Dominant modes of winter precipitation variability
766 over Central Southwest Asia and inter-decadal change in the ENSO teleconnection. *Climate*
767 *dynamics*, 53, pp.5689-5707.

768

769 Ridley, J., Wiltshire, A. and Mathison, C., 2013. More frequent occurrence of westerly disturbances
770 in Karakoram up to 2100. *Science of the Total Environment*, 468, pp.S31-S35.

771

772 Schneider, U., Becker, A., Finger, P., Meyer-Christoffer, A. and Ziese, M., 2018. GPCP full data
773 monthly product version 2018 at 0.25: monthly land-surface precipitation from rain-gauges built on
774 GTS-based and historical data. Global Precipitation Climatology Centre.

775

776 Singh, T., Saha, U., Prasad, V.S. and Gupta, M.D., 2021. Assessment of newly-developed high
777 resolution reanalyses (imdaa, ngfs and era5) against rainfall observations for indian region.
778 *Atmospheric Research*, 259, p.105679.

779

780 Syed, F.S., Giorgi, F., Pal, J.S. and Keay, K., 2010. Regional climate model simulation of winter
781 climate over Central–Southwest Asia, with emphasis on NAO and ENSO effects. *International*
782 *Journal of Climatology: A Journal of the Royal Meteorological Society*, 30(2), pp.220-235.

783

784 Tahir, A.A., Chevallier, P., Arnaud, Y. and Ahmad, B., 2011. Snow cover dynamics and hydrological
785 regime of the Hunza River basin, Karakoram Range, Northern Pakistan. *Hydrology and Earth*
786 *System Sciences*, 15(7), pp.2275-2290.

787



788 Wang, L., Chen, W., Zhou, W. and Huang, R., 2009. Interannual variations of East Asian trough axis
789 at 500 hPa and its association with the East Asian winter monsoon pathway. *Journal of Climate*,
790 22(3), pp.600-614.

791

792 Wang, S., Huang, J., He, Y. and Guan, Y., 2014. Combined effects of the Pacific decadal oscillation
793 and El Nino-southern oscillation on global land dry-wet changes. *Scientific reports*, 4(1), p.6651.

794

795 Wang, W., Matthes, K., Omrani, N.E. and Latif, M., 2016. Decadal variability of tropical
796 tropopause temperature and its relationship to the Pacific Decadal Oscillation. *Scientific reports*,
797 6(1), p.29537.

798 Wang, X., Tolksdorf, V., Otto, M. and Scherer, D., The High Asia Refined Analysis Version 2 (HAR
799 v2).

800

801 Wittenberg, A.T., Rosati, A., Delworth, T.L., Vecchi, G.A. and Zeng, F., 2014. ENSO modulation: Is
802 it decadal predictability?. *Journal of Climate*, 27(7), pp.2667-2681.

803

804 Wu, B. and Wang, J., 2002. Winter Arctic oscillation, Siberian high and East Asian winter monsoon.
805 *Geophysical research letters*, 29(19), pp.3-1.

806

807 Wu, X. and Mao, J., 2016. Interdecadal modulation of ENSO-related spring rainfall over South
808 China by the Pacific Decadal Oscillation. *Climate dynamics*, 47, pp.3203-3220.

809

810 Xie, P. and Arkin, P.A., 1997. Global precipitation: A 17-year monthly analysis based on gauge
811 observations, satellite estimates, and numerical model outputs. *Bulletin of the American
812 meteorological society*, 78(11), pp.2539-2558.

813

814 Yadav, R.K., Rupa Kumar, K. and Rajeevan, M., 2009. Increasing influence of ENSO and
815 decreasing influence of AO/NAO in the recent decades over northwest India winter precipitation.
816 *Journal of Geophysical Research: Atmospheres*, 114(D12).



817

818 Yadav, R.K., Yoo, J.H., Kucharski, F. and Abid, M.A., 2010. Why is ENSO influencing northwest
819 India winter precipitation in recent decades?. *Journal of Climate*, 23(8), pp.1979-1993.

820

821 Yadav, R.K., Rupa Kumar, K. and Rajeevan, M., 2007. Role of Indian Ocean sea surface
822 temperatures in modulating northwest Indian winter precipitation variability. *Theoretical and*
823 *applied climatology*, 87, pp.73-83.

824

825 Yamagami, Y. and Tozuka, T., 2015. Interdecadal changes of the Indian Ocean subtropical dipole
826 mode. *Climate Dynamics*, 44, pp.3057-3066.

827

828 Yang, Q., Ma, Z. and Xu, B., 2017. Modulation of monthly precipitation patterns over East China
829 by the Pacific Decadal Oscillation. *Climatic change*, 144, pp.405-417.

830

831 Yatagai, A., Kamiguchi, K., Arakawa, O., Hamada, A., Yasutomi, N. and Kitoh, A., 2012.
832 APHRODITE: Constructing a long-term daily gridded precipitation dataset for Asia based on a
833 dense network of rain gauges. *Bulletin of the American Meteorological Society*, 93(9), pp.1401-
834 1415.

835

836 Yin, J. and Zhang, Y., 2021. Decadal changes of East Asian jet streams and their relationship with
837 the mid-high latitude circulations. *Climate Dynamics*, 56, pp.2801-2821.

838

839 Yuan, X., Yang, K., Lu, H., He, J., Sun, J. and Wang, Y., 2021. Characterizing the features of
840 precipitation for the Tibetan Plateau among four gridded datasets: Detection accuracy and spatio-
841 temporal variabilities. *Atmospheric Research*, 264, p.105875.

842

843 Zhang, Y., Wallace, J.M. and Battisti, D.S., 1997. ENSO-like interdecadal variability: 1900–93.
844 *Journal of climate*, 10(5), pp.1004-1020.